

Production and Characterization of Magnesium Cement Using Kaolinite Clay

João Pedro B. Batista^{a*} , André A. S. Silva^a , Guilherme C. Cordeiro^b ,

João Claudio B. Moraes^a

^aInstituto Tecnológico de Aeronáutica (ITA), São José dos Campos, SP, Brasil.

^bUniversidade Estadual do Norte Fluminense Darcy Ribeiro (UENF), Campos dos Goytacazes, RJ, Brasil.

Received: December 17, 2022; Revised: May 28, 2023; Accepted: August 08, 2023

Magnesium silicate cement is produced by mixing reactive magnesium oxide with a source of reactive silicon oxide. This cement is an interesting alternative to Portland cement due to the potential for low energy consumption, reduced greenhouse gas emissions, and use of renewable resources. Aluminosilicate-based raw materials can also be utilized to produce this type of cement. Thus, this work aims to study the use of kaolinite clay to produce magnesium aluminosilicate cement. The cement was produced by calcination of magnesium carbonate ($MgCO_3$) and kaolinite clay at a temperature of 800 °C for 45 minutes with $MgCO_3$ /kaolin mass ratios of 90/10, 80/20, and 70/30. Mortars and pastes samples were cured at 60 °C for 1, 3, and 7 days. The results showed that the maximum compressive strength (32.7 MPa) was yielded for the 70/30 mortar mix after 3 days of curing. Microstructural studies of pastes indicated the incorporation of aluminum for the formation of magnesium aluminosilicate hydrated products, in addition to the formation of brucite.

Keywords: *Magnesium cement, kaolinite, sustainable cement.*

1. Introduction

Portland cement (PC) production emits a large amount of carbon dioxide (0.7-1.0 ton of carbon dioxide per ton of PC), consumes a high amount of non-renewable mineral resources (limestone and clay), and requires calcination at high temperature (1450 °C), reaching an energy consumption for its production of 109 kWh/t¹. In addition to environmental issues, PC has a high pH (around 13), which is harmful to some applications. As an alternative, researchers have studied a new type of cement: magnesium silicate cement.

This new cement is not usually produced by traditional clinker (calcined limestone and clay). Instead, the magnesium-based cement can be obtained by magnesite ($MgCO_3$) calcination at an average temperature of 700-900 °C, obtaining magnesium oxide (MgO), and then mixing it with a source of reactive silica (SiO_2). When hydrated, the reaction products formed are $Mg(OH)_2$ and magnesium silicate hydrate (M-S-H). This type of cement yields very satisfactory mechanical results and has a considerably less alkaline pH, which reaches values between 9 and 10²⁻⁴. Among its advantages, in addition to using magnesium carbonate calcined at low temperatures (700-900 °C) and its lower pH values (around 9-10), its use is beneficial in several applications, such as waste encapsulation radioactive materials, refractory castables, cement-based matrices for natural fibers, and aggressive environments involving $MgCl_2$ and $MgSO_4$ solutions⁵⁻⁷.

Normally, silica fume is used as a source of silicon in MgO-SiO₂ systems. However, it is an expensive and poorly

available material. In this context, calcined clays, which are rich in silica and alumina, prove to be an interesting alternative to produce this type of cement; nevertheless, only a few works have studied this type of cement. Bernard et. al⁸ have investigated the aluminum influence on magnesium silicate hydrate, and authors confirmed that aluminum can be incorporated into its structure to form M-A-S-H type products. Dhakal et. al⁹ produced the magnesium-silicate binder system using industrial MgO (Mg) and metakaolin (Mk) as a silica source, and the samples yielded a compressive strength of 50 MPa with a 1.25 Mg/Mk mass ratio.

The aim of this study is to present a new production methodology with the calcination of the raw materials in a furnace at 800 °C for 45 minutes to produce magnesium silicate cement using magnesium carbonate and kaolin, a material with high availability at low cost as a source of silicon and aluminum oxides.

2. Materials and Methods

The raw materials, magnesium carbonate ($MgCO_3$) and kaolin, were obtained from Brasilminas. Siliceous sand was used as fine aggregate (fineness modulus of 2.50 and apparent specific gravity of 2.42). Superplasticizer ViscoCrete HE-20 was supplied by Sika. The particle size distribution (Mastersizer 3000 Malvern equipment) of the raw materials was assessed and its chemical composition was sourced by Brasilminas.

In the production of magnesium aluminosilicate cement, the $MgCO_3$ and kaolin were homogenized in a ball mill for 30 minutes. The mixture was calcined in a laboratory furnace (18 kW, 200 L) for 45 minutes at a temperature of 800 ± 15 °C.

*e-mail: jpdrobb92@gmail.com

After, the generated cement was cooled in the open air, and then it was homogenized in a ball mill for 30 minutes. The MgCO_3 /kaolin mass proportions used were 90/10, 80/20, and 70/30. For characterization of magnesium aluminosilicate cements, the samples were assessed by X-ray diffraction (XRD, PANalytical Empyrean diffractometer equipped with an X'Celerator detector, Bragg Angle interval of 10–70°, Cu-K α radiation, Ni filter, step of 0.01° and 10 s/step), Fourier transform infrared-attenuated total reflectance spectroscopy (FTIR-ATR, PerkinElmer spectrophotometer, spectrum range of 4000–400 cm^{-1} and spectral resolution of 1 cm^{-1}) and scanning electron microscopy coupled with energy-dispersive X-ray spectroscopy (SEM/EDS, TESCAN VEGA 3 XMU equipment, Oxford EDS 133 eV detector).

Mortars and pastes were produced to assess the compressive strength and microstructure, respectively. The water/binder mass ratio was 0.55, the fine aggregate/binder mass ratio (for mortars) was 2.00, and the mass of superplasticizer addition was 4% by mass of binder. The compressive strength of 40-mm cubic specimens was assessed after 1, 3, and 7 days of curing at 60 °C in a universal testing machine (600 kN-load limit and load rate of 0.5 kN/s). Microstructural studies of pastes were analyzed by means of XRD, FTIR, and SEM/EDS tests with the same parameters as the raw materials and anhydrous cement characterization. In the case of XRD and FTIR, the tests were performed for powdered samples; whereas, in the case of SEM/EDS, the test was performed for fractured samples with flat surface.

The nomenclature of the cements, pastes, and mortars are presented, respectively, in the “C-x/y”, “P-x/y”, and “M-x/y” formats, in which “x” is the value of the mass proportion of MgCO_3 and “y” is related to the mass proportion of kaolin.

Table 1 summarizes the information on the raw materials, magnesium aluminosilicate cements, pastes, and mortars.

3. Results and Discussion

Table 2 shows the chemical composition, bulk density, and mean particle size of MgCO_3 and kaolin. The magnesium carbonate is mainly composed by MgO (47.68 wt.%), has a bulk density of 2.9 g/cm^3 , and presents a mean particle size of 21.0 μm . The kaolin is mainly composed of SiO_2 (45.50 wt.%) and Al_2O_3 (34.50 wt.%). Its bulk density is 2.5 g/cm^3 and the mean particle size is 10.3 μm .

Figure 1 shows XRD patterns of raw materials (MgCO_3 and kaolin) and magnesium aluminosilicate cements 90/10 (C-90/10), 80/20 (C-80/20), and 70/30 (C-70/30). Respect to raw materials, the crystalline phase detected for MgCO_3 was magnesite (MgCO_3 , PDF Card 0000099); whereas, for kaolin, kaolinite ($2\text{SiO}_2 \cdot \text{Al}_2\text{O}_3$, PDF Card 0020861), illite ($(\text{K}, \text{H}_3\text{O})(\text{Al}, \text{Mg}, \text{Fe})_2(\text{Si}, \text{Al})_4\text{O}_{10}(\text{OH})_2(\text{H}_2\text{O})$, PDF Card 0005017), and quartz (SiO_2 , PDF Card 0000789) were identified. Regarding the cements, quartz and periclase (MgO , PDF Card 0000501) were detected as crystalline phases. Figure 2 presents the FTIR spectra of raw materials and magnesium aluminosilicate cements 90/10, 80/20, and 70/30. With respect to raw materials, the identified bands for MgCO_3 were 1437, 882, and 746 cm^{-1} (O-C-O asymmetric stretching mode); whereas, for kaolin, the detected bands were 525 and 794 cm^{-1} (Si-O-Si/Al bending mode), at 680 cm^{-1} and in the range of 910–1115 cm^{-1} (Si-O-Si/Al stretching mode), and at 3690 cm^{-1} (O-H stretching mode)¹⁰. Regarding the cements, some differences could be observed with respect to the raw materials: the formation of the band in 600 cm^{-1} - 400 cm^{-1} region due to MgO formation; the band position

Table 1. Information on the sample types raw materials, anhydrous cement, paste and mortar: sample name, raw materials mass proportions, water/binder and fine aggregate/binder ratios, curing time and temperature, and tests performed.

Sample type	Sample name	MgCO_3 / kaolin mass proportion	Water / binder mass ratio	Fine aggregate / binder mass ratio	Curing time and temperature	Tests					
						Chemical composition	Bulk density	Particle size diameter	XRD	FTIR	SEM /EDS
Raw materials	MgCO_3	N.A.	N.A.	N.A.	N.A.	x	x	x	x	x	
	Kaolin					x	x	x	x	x	
Anhydrous cement	C-90/10	90/10	N.A.	N.A.	N.A.				x	x	
	C-80/20	80/20							x	x	x
	C-70/30	70/30							x	x	
Paste	P-90/10	90/10	0.55	N.A.	3 days at 60 °C				x	x	x
	P-80/20	80/20							x	x	x
	P-70/30	70/30							x	x	x
Mortar	M-90/10	90/10	0.55	2.00	1, 3 and 7 days at 60 °C						x
	M-80/20	80/20									x
	M-70/30	70/30									x

Table 2. Chemical composition, bulk density, and mean particle size of MgCO_3 and kaolin.

Raw material	Chemical Composition (wt.%)								Bulk density (g/cm^3)	Mean particle size (μm)
	MgO	CaO	Fe_2O_3	Al_2O_3	SiO_2	K_2O	Na_2O	LOI*		
MgCO_3	47.68	0.43	0.14	0.03	0.21	-	-	51.51	2.9	21.0
Kaolin	0.49	-	0.23	34.50	45.5	0.55	0.32	18.41	2.5	10.3

*LOI: Loss on ignition

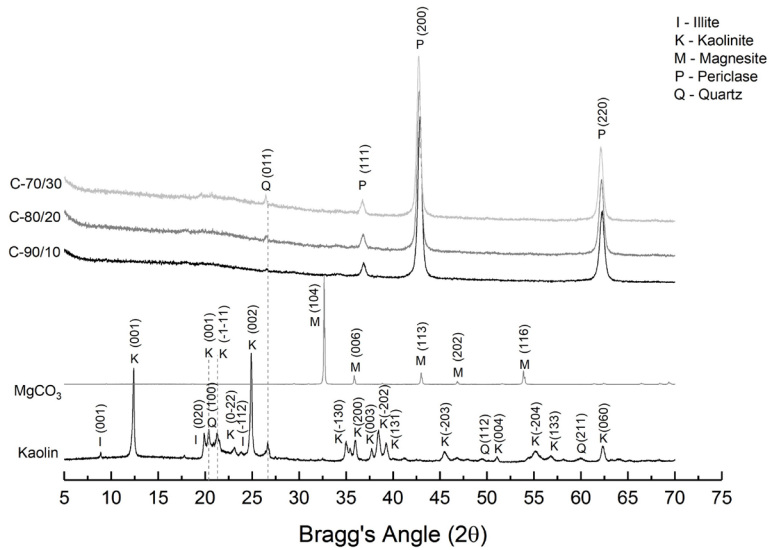


Figure 1. XRD patterns of raw materials ($MgCO_3$ and kaolin) and magnesium aluminosilicate cements 90/10 (C-90/10), 80/20 (C-80/20), and 70/30 (C-70/30).

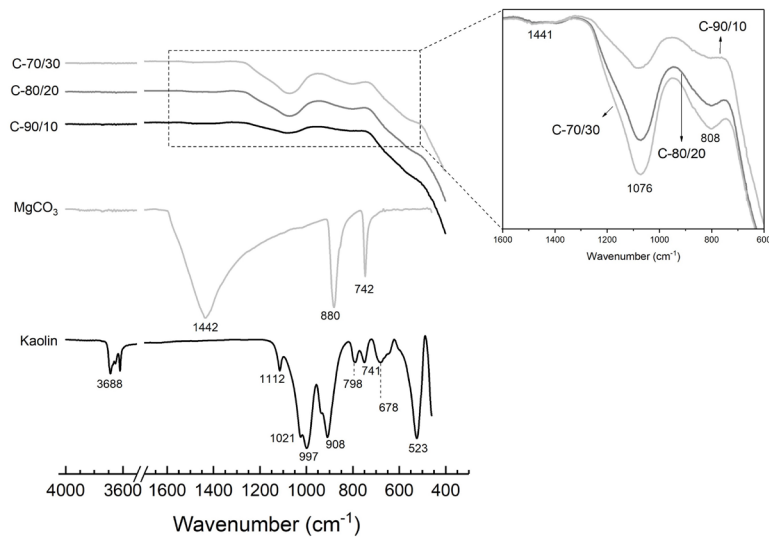


Figure 2. FTIR spectra of raw materials ($MgCO_3$ and kaolin) and magnesium aluminosilicate cements 90/10 (C-90/10), 80/20 (C-80/20), and 70/30 (C-70/30).

at $1200-800\text{ cm}^{-1}$ has shifted in relation to raw materials; the band at 1400 cm^{-1} disappeared due to decarbonation of $MgCO_3$ to form MgO ; and finally, the band at 3600 cm^{-1} disappeared due to kaolin dihydroxylation. Figure 3 shows the SEM/EDS of the 80/20 cement sample. Two different particle morphologies were detected: one with a larger size and with a flat surface attributed to MgO particles, and another with an irregular shape attributed to kaolin particles, confirmed by EDS mapping.

Figure 4 shows compressive strengths of mortars M-90/10, M-80/20, and M-70/30 after 1, 3, and 7 days of curing. Results showed that the optimum magnesium aluminosilicate cement was 70/30 after 3 days of curing, which yielded a compressive strength of 32.7 MPa. In addition, it could be noted that the values of compressive strength decreased at 7 days. This

result agrees with Sonat et. al¹¹, which observed a rapid gain in compressive strength values at early ages due to the acceleration of the dissolution of MgO and SiO_2 , increasing M-S-H formation. However, the decrease in strength at ages higher than 3 days was due to instability and the potential disintegration of M-S-H after losing its interlayer water at high temperatures. Figure 5 shows the XRD patterns of pastes P-90/10, P-80/20, and P-70/30 after 3 days of curing at 60°C . The identified crystalline phases attributed to reaction products were brucite ($Mg(OH)_2$, PDF Card 0001637), hydrotalcite ($Mg_6Al_2(OH)_2(OH)_6 \cdot 3H_2O$, PDF Card 0014738), and magnesium silicate hydrate-like reaction product (M-S-H). In addition, Figure 6 shows the FTIR spectra of pastes P-90/10, P-80/20, and P-70/30 after 3 days of curing. The detected FTIR spectra bands for all pastes were 1012 cm^{-1} (Si-O-Si/Al

stretching mode), 1388 cm^{-1} (O-C-O asymmetric stretching mode), and 1637 cm^{-1} (O-H bending mode). Moreover, a peak at 3690 cm^{-1} (O-H stretching mode) was also identified. Brucite was identified in magnesium silicate cement due to the hydration of MgO, as shown in the XRD pattern and FTIR spectra (band at 1637 cm^{-1} and peak at 3690 cm^{-1}). The presence of Al and Mg in the composition of cement leads to the formation of hydrotoalcite, as identified in the XRD pattern and FTIR spectra (band at 1388 cm^{-1}). M-S-H-like reaction

product (probably M-A-S-H) presents a great tendency to form with the increase of $\text{SiO}_2/\text{Al}_2\text{O}_3$ content, and it was also identified in XRD pattern and FTIR spectra (shifting of the band at 1076 cm^{-1} from the anhydrous cement to 1012 cm^{-1} in pastes). Formation of M-A-S-H hydration products can result in densified microstructure, leading to suitable compressive strength. However, in a previous study with MgO-SiO_2 , an increase in M-S-H products not necessarily increased compressive strength^{12,13}.

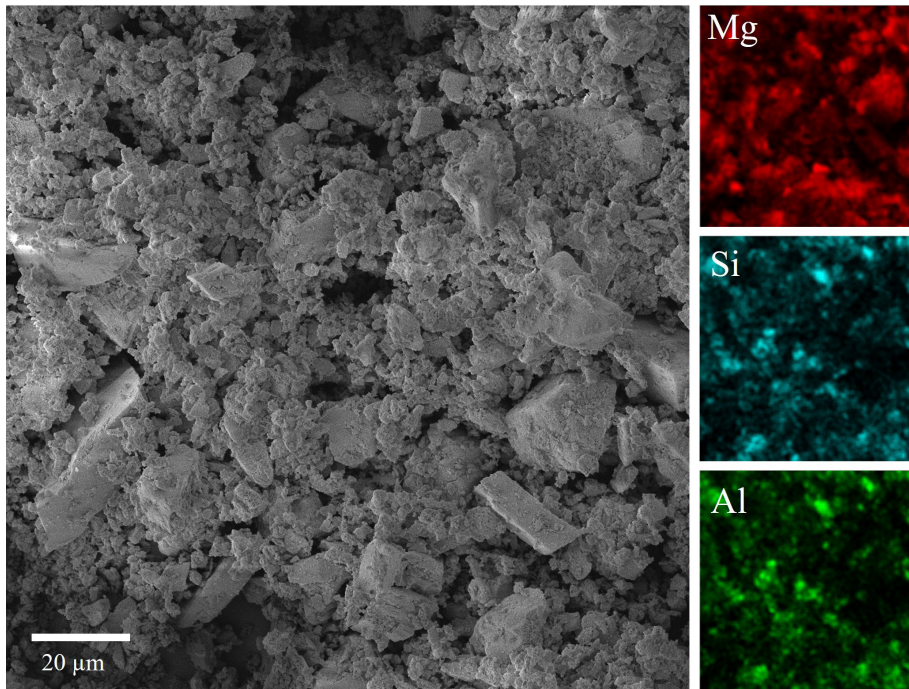


Figure 3. SEM image and EDS results of 80/20 cement (C-80/20).

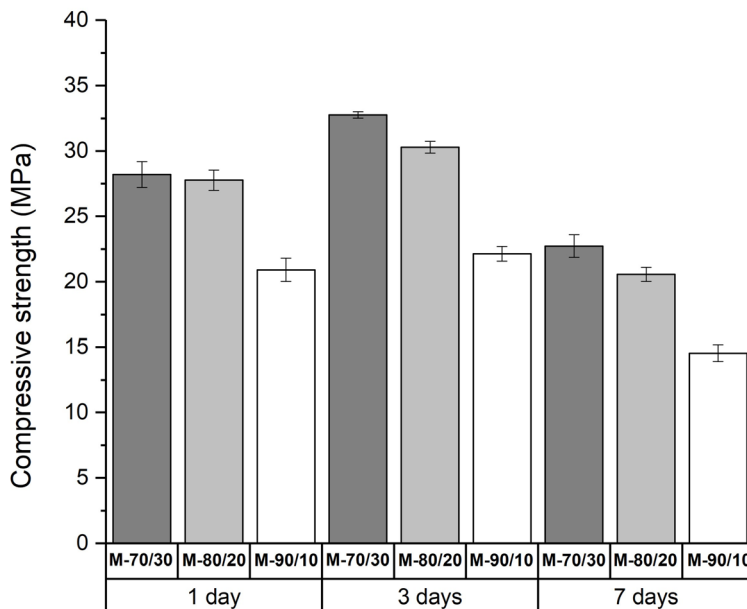


Figure 4. Compressive strength of mortars M-70/30, M-80/20, and M-90/10 after 1, 3, and 7 days of curing at $60\text{ }^{\circ}\text{C}$.

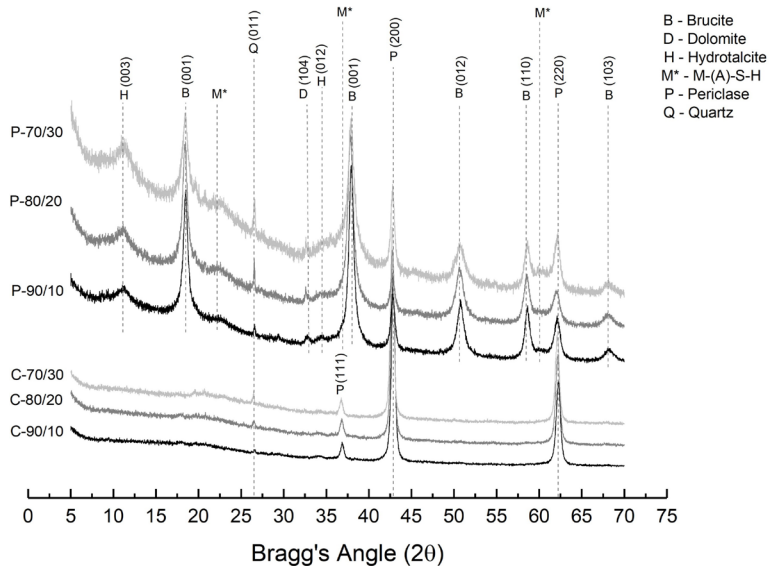


Figure 5. XRD patterns of P-70/30, P-80/20, and P-90/10 pastes after 3 days of curing at 60 °C.

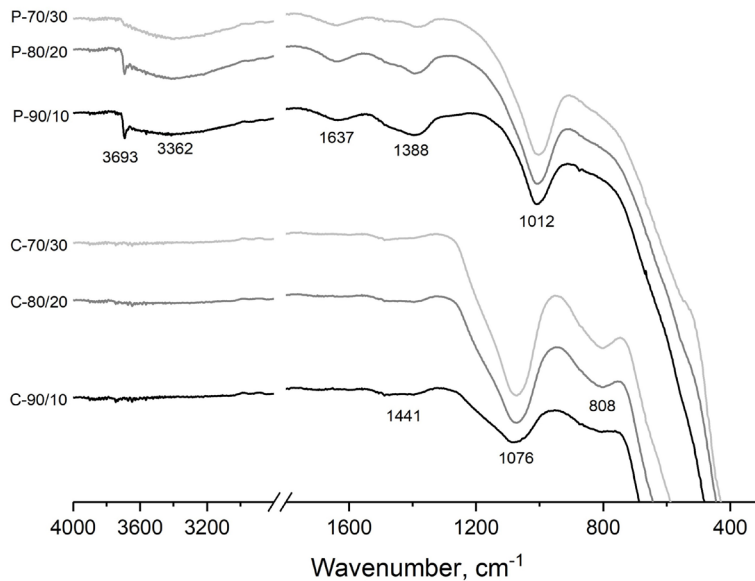


Figure 6. FTIR spectra of P-70/30, P-80/20, and P-90/10 pastes after 3 days of curing at 60 °C.

Figure 7 shows the SEM images and EDS results for 90/10 (P-90/10), 80/20 (P-80/20), and 70/30 (P-70/30) pastes after 3 days of curing. It can be observed in the images with higher magnification (Figure 7d-f), that the P-80/20 and P-70/30 samples presented denser microstructure. In general, two types of structure can be seen, one with a more defined shape and smooth surfaces, attributed to brucite (identified as C, E, and H in Figure 7) and kaolinite (identified as B, F, and I in Figure 7) particles. In the another structure, a denser and more continuous shape was attributed to M-A-S-H product (identified as A, D, and G in Figure 7). The identification of the structures was based on the mean atomic content and atomic ratios by the semi-quantitative results of EDS

test, which is shown in Table 3. The structure identified as brucite presented the highest values for the Mg/(Si+Al) ratio (7.4-13.1). On the other hand, the M-A-S-H product showed a variation of 0.7-1.6 for the Mg/(Si+Al) ratio. Finally, for the kaolinite particles, the ratio Mg/(Si+Al) was 0.2. It is important to highlight that the lower the amount of MgO in the cement, the greater the amount of silicon and aluminum in the M-A-S-H product.

4. Conclusions

The calcination process utilized for MgCO₃/kaolin mass ratios of 90/10, 80/20, and 70/30 resulted in magnesium

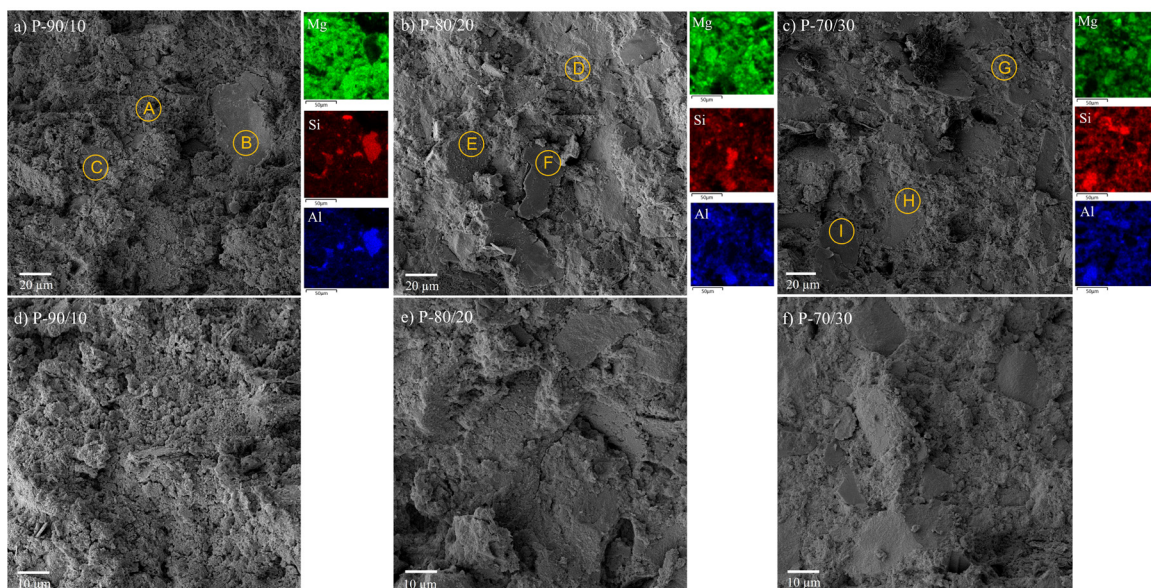


Figure 7. SEM/EDS images of P-90/10 (a and d), P-80/20 (b and e) and P-70/30 samples (c and e).

Table 3. Semi-quantitative mean atomic content (in %) and atomic ratios of pastes P-90/10, P-80/20, and P-70/30 after 3 days of curing at 60 °C (spots indicated in the Figure 7).

Spot	Element (in atomic percentage, at.%)			Atomic ratios		Identification
	Mg	Si	Al	Mg/(Si+Al)		
A	61.4	24.6	14.0	1.6		M-A-S-H
B	19.1	43.5	37.4	0.2		Calcined kaolin particle
C	91.5	6.1	2.4	10.8		Brucite
D	59.3	19.5	21.2	1.5		M-A-S-H
E	88.1	7.2	4.7	7.4		Brucite
F	15.5	47.1	37.4	0.2		Calcined kaolin particle
G	41.7	32.7	25.6	0.7		M-A-S-H
H	92.9	5.7	1.4	13.1		Brucite
I	18.0	44.2	37.8	0.2		Calcined kaolin particle

aluminosilicate cements with suitable properties. Compressive strength results indicated that the optimum $\text{MgCO}_3/\text{kaolin}$ mass ratio was 70/30, yielding 32.7 MPa after 3 days of curing at 60 °C. The XRD test indicated that the calcination process was effective due to the absence of kaolinite and the formation of periclase in the cements. The EDS test confirmed that the aluminum atoms were incorporated to form M-A-S-H gels. Microstructural studies of pastes showed the formation of the following reaction products: M-A-S-H, $\text{Mg}(\text{OH})_2$, and hydrotalcite. Finally, this work enables the validation of low-energy cement using kaolin as a source of aluminosilicate.

5. Acknowledgments

This work was supported by Coordenação de Aperfeiçoamento de Pessoal de Nível Superior (CAPES) for the scholarship, and for research project grant (Process CNPq 425675/2018-1). We thank SIKA for providing superplasticizer; Laboratório de Plasmas e Processos, Instituto Tecnológico de Aeronáutica, Brazil, for providing analysis on X-ray Diffractometer and Fourier-Transform Infrared Spectrometers equipment; Materials

and Processes Department, Mechanical Engineering Division, Instituto Tecnológico de Aeronáutica, Brazil, for SEM/EDS equipment; and Laboratório de Análises Instrumentais, Divisão de Propulsão, Instituto de Aeronáutica e Espaço, Brazil, for providing particle size characteristics.

6. References

1. Tan Y, Yu H, Sun S, Wu C, Ding H. Properties and microstructure of basic magnesium sulfate cement: influence of silica fume. *Constr Build Mater.* 2021;266:121076. <http://dx.doi.org/10.1016/j.conbuildmat.2020.121076>.
2. Zhang T, Cheeseman CR, Vandeperre LJ. Development of low pH cement systems forming magnesium silicate hydrate (M-S-H). *Cement Concr Res.* 2011;41(4):439-42. <http://dx.doi.org/10.1016/j.cemconres.2011.01.016>.
3. Jin F, Al-Tabbaa A. Thermogravimetric study on the hydration of reactive magnesia and silica mixture at room temperature. *Thermochim Acta.* 2013;566:162-8. <http://dx.doi.org/10.1016/j.tca.2013.05.036>.
4. Sonat C, Dung NT, Unluer C. Performance and microstructural development of MgO-SiO_2 binders under different curing conditions. *Constr Build Mater.* 2017;154:945-55. <http://dx.doi.org/10.1016/j.conbuildmat.2017.08.020>.

5. Sonat C, Unluer C. Development of magnesium-silicate-hydrate (M-S-H) cement with rice husk ash. *J Clean Prod.* 2019;211:787-803. <http://dx.doi.org/10.1016/j.jclepro.2018.11.246>.
6. Mármol G, Savastano H Jr. Study of the degradation of non-conventional MgO-SiO₂ cement reinforced with lignocellulosic fibers. *Cement Concr Compos.* 2017;80:258-67. <http://dx.doi.org/10.1016/j.cemconcomp.2017.03.015>.
7. Mármol G, Savastano H Jr, Tashima MM, Provis JL. Optimization of the MgO SiO₂ binding system for fiber-cement production with cellulosic reinforcing elements. *Mater Des.* 2016;105:251-61. <http://dx.doi.org/10.1016/j.matdes.2016.05.064>.
8. Bernard E, Lothenbach B, Cau-Dit-Coumes C, Pochard I, Rentsch D. Aluminum incorporation into magnesium silicate hydrate (M-S-H). *Cement Concr Res.* 2020;128:105931. <http://dx.doi.org/10.1016/j.cemconres.2019.105931>.
9. Dhakal M, Scott AN, Shah V, Dhakal RP, Clucas D. Development of a MgO-metakaolin binder system. *Constr Build Mater.* 2021;284:122736. <http://dx.doi.org/10.1016/j.conbuildmat.2021.122736>.
10. Li Z, Yu Q, Chen X, Liu H, Zhang J, Zhang J, et al. The role of MgO in the thermal behavior of MgO-silica fume pastes. *J Therm Anal Calorim.* 2017;127(3):1897-909. <http://dx.doi.org/10.1007/s10973-016-5827-6>.
11. Sonat C, Dung NT, Unluer C. Performance and microstructural development of MgO-SiO₂ binders under different curing conditions. *Constr Build Mater.* 2017;154:945-55. <http://dx.doi.org/10.1016/j.conbuildmat.2017.08.020>.
12. Jin F, Al-Tabbaa A. Strength and hydration products of reactive MgO-silica pastes. *Cement Concr Compos.* 2014;52:27-33. <http://dx.doi.org/10.1016/j.cemconcomp.2014.04.003>.
13. Tran HM, Scott A. Strength and workability of magnesium silicate hydrate binder systems. *Constr Build Mater.* 2017;131:526-35. <http://dx.doi.org/10.1016/j.conbuildmat.2016.11.109>.